Interaction of cavity solitons on an unstable background

Interaction of cavity solitons on an unstable background

Shayesteh Rahmani Anbardan,[1,*] Cristina Rimoldi,[2] Reza Kheradmand,[1,3] Giovanna Tissoni,[4] and Franco Prati[5]

[1]*Photonics group, Research Institute for Applied Physics & Astronomy, University of Tabriz, Tabriz, Iran*

[2]*INRS-EMT, 1650 Boulevard Lionel-Boulet, Varennes, Québec, Canada J3X 1S2*

[3]*Photonics and Plasma technology group, Faculty of Physics, University of Tabriz, Tabriz, Iran*

[4]*Université Côte d'Azur, Institut de Physique de Nice, 1361 route des Lucioles, 06560 Valbonne, France*

[5]*Dipartimento di Scienza e Alta Tecnologia, Università dell'Insubria, Via Valleggio 11, 22100 Como, Italy*

(Received 19 July 2019; accepted 19 February 2020; published 16 April 2020)

The interaction of two cavity solitons in a driven semiconductor laser above lasing threshold is investigated. We focus on the case in which the background field of the solitons is turbulent because the laser is below the injection locking point. We show that the solitons move spontaneously and either reach some equilibrium distance or merge. Different behaviors are found depending on how far from the injection locking point the laser is. The laser is modeled by a set of effective Maxwell-Bloch equations which include an equation for the macroscopic polarization that mimics the complex susceptibility of the semiconductor. In that way we avoid the emergence of an unphysical behavior of the background which instead appears when the polarization is adiabatically eliminated, which amounts to assuming infinite gain linewidth. The simulations are slow because the time scales of the different dynamical variables differ by four orders of magnitude. Yet, we show that the results of the complete set of equations can be accurately reproduced with a reduced set of equations where the polarization is adiabatically eliminated but a diffusion term is included in Maxwell equation, which accounts for the finiteness of the gain linewidth.

DOI: 10.1103/PhysRevE.101.042210

I. INTRODUCTION

Semiconductor lasers are very sensitive to external perturbations, i.e., optical injection and external optical feedback due to a combination of intrinsic, material-related properties leading to relaxation oscillations and self-phase modulation. Such instabilities are manifestations of highly complex structures of nonlinear dynamics and bifurcations [1,2]. It is also well known that in broad area vertical cavity surface emitting lasers (VCSELs) with external optical injection, complex spatial patterns and cavity solitons (CSs) can be formed due to the interplay among dispersive or absorptive nonlinearities, paraxial diffraction, dissipation and feedback [3,4].

CSs, or autosolitons, were initially predicted in a bistable nonlinear resonator containing a two-level instantaneous medium [5]. With the aim of modeling experiments performed with a driven VCSEL, a more refined model was then introduced which accounts for the properties of the semiconductor medium by including phase-amplitude coupling through the α factor in the equation for the electric field and coupling it with an equation for the slow gain [6,7]. Such a model can be thought of as the rate equation limit of a Maxwell-Bloch-like set of equations where the material polarization P is adiabatically eliminated. The model was applied successfully to the first experimental demonstration of CSs in a broad area VCSEL slightly below the lasing threshold [8,9]. In the experiment the VCSEL was pumped above transparency, so that it acted as an amplifier, but slightly below the lasing threshold, which means that the gain experienced by light in the amplifier was not sufficient to overcome cavity losses and the VCSEL would not emit light unless it was driven by an external coherent field.

When the laser is above threshold, however, a competition arises between the lasing frequency and the frequency of the injected field, which results in an oscillatory instability as long as the amplitude of the injected field is below a critical value which marks the injection locking point. Above that critical value the laser is locked to the external frequency. In a spatially extended system, the oscillations below the injection locking point affect also the transverse modes of the electric field, giving rise to complex spatiotemporal dynamics, or turbulence. In that case, it was shown that the simple adiabatic elimination of the polarization variable is not correct because below the injection locking point it leads to oscillatory instabilities with a spuriously high critical wave number [10]. For that reason a set of effective semiconductor Maxwell-Bloch equations that includes an equation for the macroscopic polarization was used by Hachair *et al.* [11] to model the first experiment where CSs were observed in a driven VCSEL above lasing threshold. It was found that a Hopf instability, typical of driven lasers above threshold, affects the lower intensity branch of the homogeneous steady state, while the higher intensity branch is unstable due to a Turing instability. In agreement with the experimental findings the model predicts that CSs exist and are stable even when the lower branch of the bistable curve is unstable, although the CSs are no longer stationary and display irregular intensity and phase oscillations, due to the turbulence of the background [11,12].

*rahmani. a.shayesteh@gmail.com

A relevant feature of CSs is that in a transversally homogeneous optical cavity they are marginally stable with respect to translations. A neutral mode therefore exists, associated to translational symmetry [13,14]. In a laser with saturable absorber, where CSs exist even in the absence of optical injection, this property of CSs allows various kinds of motion, spanning from spontaneous motion in the presence of a drift instability for CS as in Refs. [15,16] to CS motion related to the formation of CS complexes as in Refs. [17,18]. Moreover, in the same system, interesting CS trajectories are also predicted in the case of collisions between moving CS and interactions of moving CS with material defects, such as peaks or wells in the carrier density due to inhomogeneities in the injected current [19]. Here, however, we are interested in lasers without a saturable absorber and driven by an external field, also named the holding beam. In that case the motion of CSs can be both spontaneous and induced by gradients in the holding beam itself.

It was shown that in the presence of an amplitude gradient CSs tend to move towards the nearest local maximum of intensity of the holding beam [7]. This perhaps undesired effect can be compensated by phase modulations in the holding beam which allow one to fix the positions of the solitons by means of a phase mask, as shown numerically in Ref. [7] and experimentally in Ref. [20].

A constant phase gradient instead makes CSs move at a constant velocity, proportional to the gradient amplitude [13]. This property makes it possible to realize a delay line using cavity solitons that drift laterally with typical velocities on the order of 1 km/s [21]. The above examples refer to a coherently driven VCSEL below the lasing threshold. In the case of a coherently driven VCSEL above threshold an ultrafast delay line has been numerically demonstrated in Ref. [22].

On the other hand, spontaneous motion of cavity solitons can be induced by thermal effects [23,24]. This slow drift can be controlled again by using a holding beam with amplitude or phase modulations [25].

More recently, another kind of spontaneous motion was demonstrated numerically in a VCSEL above lasing threshold, which occurs when two CSs are excited in different positions. The two solitons move one towards the other over long time scales due to an attractive force with which an exponentially decaying interaction potential can be associated [26]. No matter how distant initially the two CSs are, they eventually merge, and the merging time increases exponentially with the initial distance. In Ref. [26] the laser was operated above the lasing threshold and *above* the locking point, and consequently the CSs have a stable background.

In this paper we consider the interaction of two CSs when the laser is above lasing threshold as before, but it is now operated *below* the injection locking point, so that CSs sit over an unstable background which induces intensity and phase oscillation in the CSs themselves [11]. We show that the behavior is quite different from that observed in Ref. [26], because here, instead of merging, the CSs move and typically reach an equilibrium distance before they stop, unless they are initially very close to each other.

We also show that the adiabatic elimination of the polarization variable, which was possible in Ref. [26] because of the absence of oscillatory instabilities, here produces results that are substantially different from those of the full model. Yet, it is enough to add to the equation for the electric field a diffusion term, which acts as a spectral filter, to recover a behavior very similar to that of the complete model.

The interest in this study is not purely academic, in that the mechanism of soliton merging can be viewed as a means to realize an optical AND gate [22].

It is interesting to recall here that, instead of merging, CSs in a *passive resonator* may form stable clusters at some preferred separation distances, as shown for instance in Refs. [5,27,28]. In those examples, single localized structures are found to have oscillatory decaying tails, originating from diffraction. Numerical simulations [27] and analytical prediction based on the asymptotic form of the soliton tails [28] show that the corresponding CS interactions are mediated by their oscillatory tails and make it possible to predict the actual separation among CSs in a cluster. Interesting interaction properties of dissipative solitons and, in particular, their locking at preferred distances have been also recently shown for the case of oscillating localized structures in a driven Kerr medium [29] or in a semiconductor laser with saturable absorber [30].

In Sec. II we introduce the dynamical equations and find the stable CSs branch below and above the locking point, in Sec. III we analyze the dynamical behavior of two interacting CSs for different values of the holding beam intensity, and in Sec. IV we discuss the validity of reduced models where the polarization P is adiabatically eliminated and a diffusion term is added or not in the equation for the electric field. The conclusions are drawn in the final section.

II. MODEL

We consider a VCSEL-type laser which contains a multiple quantum well structure as the active medium. The laser is pumped above lasing threshold and it is driven by a broad area and stationary holding beam. The spatiotemporal dynamics of the laser can be modeled by the effective semiconductor Maxwell-Bloch equations [11,31]

$$\dot{E} = \sigma[E_{HB} - (1 + i\theta)E + P + i\nabla^2 E], \tag{1}$$

$$\dot{D} = \mu - D - (E^* P + P^* E)/2 + d_D \nabla^2 D, \tag{2}$$

$$\dot{P} = \xi(D)[(1 - i\alpha)D(1 - \beta D)E - P], \tag{3}$$

where E and P are the cavity field and the macroscopic semiconductor polarization variables, respectively, D is carrier density, σ is the scaled photon decay rate, E_{HB} is the amplitude of the holding beam, θ is the detuning between cavity and optical injection, α is the linewidth enhancement factor, μ is the pump parameter, d_D is the carrier diffusion constant, and β is the nonlinear gain coefficient.

Diffraction is described by the Laplacian operator, ∇^2, and the spatial variables are scaled to the square root of the diffraction parameter (typically of the order of 4–5 μm). Time is scaled to the carrier decay time, which is assumed to be 1 ns. Assuming also that the photon lifetime in the cavity is about 2.5 ps, the scaled photon decay rate is $\sigma = 400$.

The complex function $\xi(D)$ is defined as $\xi(D) = \Gamma(D)(1 - i\alpha) + 2i\delta(D)$ and the two real functions $\Gamma(D)$ and

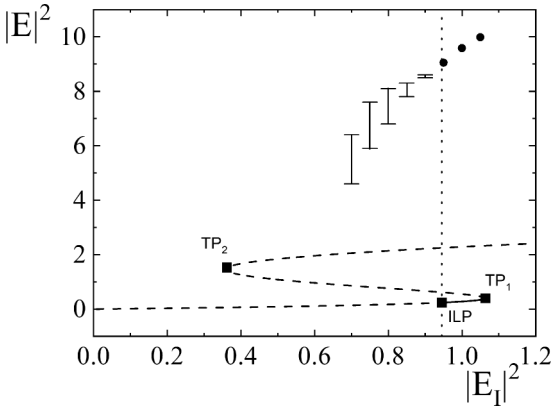

FIG. 1. Homogeneous stationary solution (solid and dashed lines) and stable branch of CSs (error bars and circles) for $\alpha = 4$, $\theta = -2$, $\beta = 0.125$, $\mu = 1.2\mu_{th}$, $\sigma = 400$, and $d_D = 0.052$. The homogeneous stationary solution is unstable in the lower branch from the origin to the injection locking point (ILP) due to a Hopf instability, in the negative slope branch between the two turning points TP_1 and TP_2, and in the upper branch from the turning point TP_2 in all the visible range due to a Turing instability. It is stable only in the small portion of the lower branch between ILP and TP_1. The vertical dotted lines passing through ILP mark the boundary between stable, stationary CSs with stable background (circles) and stable CSs with a turbulent background. The peak intensity of the latter oscillates between the limits of the vertical bar.

$\delta(D)$ account for the dependence on the carrier density of the effective semiconductor susceptibility. In particular, $\Gamma(D)$ is associated with the gain linewidth and $\delta(D)$ is the detuning between the reference frequency and the frequency where gain is maximum. In this paper, we set $\Gamma(D) = (0.560D + 0.293) \times 10^4$ and $\delta(D) = (0.155D - 0.146) \times 10^4$ [11,22]. The value of the nonlinear gain coefficient β that we use here is $\beta = 0.125$. It is obtained as the best fit of the gain calculated with the microscopic model. For this value of β, the lasing threshold current is $\mu_{th} = 1.17$. The other parameters are $\alpha = 4$, $\theta = -2$, $\mu = 1.2\mu_{th}$, and $d_D = 0.052$. For this choice of the parameters, the homogeneous stationary solution, obtained by setting $\partial_t E = 0$, $\nabla^2 E = 0$, is S shaped, as shown in Fig. 1. The only stable part of this curve is the small portion of the lower branch represented with a solid line. The dashed part of the lower branch is Hopf unstable up to the injection locking point. The negative slope branch is unstable as usual, for a stationary instability, and the upper branch is modulationally (Turing) unstable in the range shown in the figure.

By use of a split-step method with periodic boundary conditions in the transverse plane, the full set of dynamical equations (1)–(3) including the polarization equation were integrated numerically.

Stable CSs exist in the interval 0.7–1.05 of the holding beam intensity, which includes the locking point, which is $|E_I|^2 = 0.945$, $|E|^2 = 0.239$. Therefore, CSs can be excited in the Hopf unstable region before the locking point, where they coexist with an unstable background and display random intensity oscillations whose amplitude depends on the intensity of the holding beam [31]. As we move away from the locking point the amplitude of the oscillations increases, as shown in Fig. 1. We notice that the CSs do not undergo a different Hopf instability than the homogeneous stationary solution: they display irregular oscillations just below the injection locking point where the homogeneous stationary solution is turbulent.

To write the CSs two Gaussian address beams of width w and amplitude E_0 centered at (x_i, y_i), $i = 1, 2$ are superimposed to the holding beam during a short time interval τ_{inj} so that we replace the holding beam E_{HB} in Eq. (1) with the total injected field

$$E_I(x, y, t) = E_{HB} + f(t) \sum_{i=1}^{2} E_0 e^{-[(x-x_i)^2+(y-y_i)^2]/2w^2}, \quad (4)$$

where $f(t) = 1$ for $t \leqslant \tau_{inj}$ and $f(t) = 0$ for $t > \tau_{inj}$.

III. INTERACTION OF CAVITY SOLITONS

Initially we study the dynamics of interacting CSs using the complete set of Eqs. (1)–(3), in order to avoid the unphysical effects that could arise from the adiabatic elimination of the macroscopic polarization P, as commented in the Introduction. We write simultaneously two CSs in positions symmetric with respect to the center of VCSEL's section, either along a diagonal or along a horizontal line. We let them evolve and interact until they merge or they reach a constant distance.

We study the interaction of CSs which are excited just below the Hopf bifurcation point of the homogeneous stationary solution ($|E_{HB}|^2 = 0.9$), and in the middle of the Hopf region ($|E_{HB}|^2 = 0.75$) where the intensity oscillations of the CSs are large. The injection parameters suitable to write the CS are $E_0 = 1$ and $w = 1$, and injection must last 3 ns for $|E_{HB}|^2 = 0.9$ and 4 ns for $|E_{HB}|^2 = 0.75$.

In the numerical integration we used a 64×64 spatial grid, but then, using the Fourier amplitudes of the field E obtained in the dynamical simulation, we calculate the field E on a larger grid 640×640. In that way we can follow the motion of the CSs with a better resolution. Since the space step for the 64×64 grid is 0.5 spatial units (s.u.), the resolution is 0.05. Assuming that a spatial unit is 4 μm, we can follow the motion of the CSs on a spatial grid with period 0.2 μm.

Figure 2 shows the interaction of CSs just below the locking point, for $|E_{HB}|^2 = 0.9$. The time evolution of the distance of the CSs is shown in panel (a) and the trajectory of the CSs in the transverse plane x, y in panel (b).

For the smallest initial distances, up to 12 s.u., the behavior is similar to that observed above the locking point, when the background is stable [26]. The two CSs attract each other and they move faster and faster until they merge into one at the center. As in Ref. [26], the merging time increases exponentially with the initial distance. Yet, different from [26], the motion does not occur on a straight line, as a consequence of the unstable background. This is shown in Fig. 2(b) for the initial distance 12 s.u. (green line).

For larger initial distances, between 13 and 21.21 s.u., the two CSs get closer but they do not merge any longer and they move until they reach an equilibrium distance equal to 11.4 s.u. In Fig. 2(b) we show the trajectories for the initial distance 21.21 s.u. (red line) and 13 s.u. (blue line). For the larger initial distance the two CSs at the beginning move

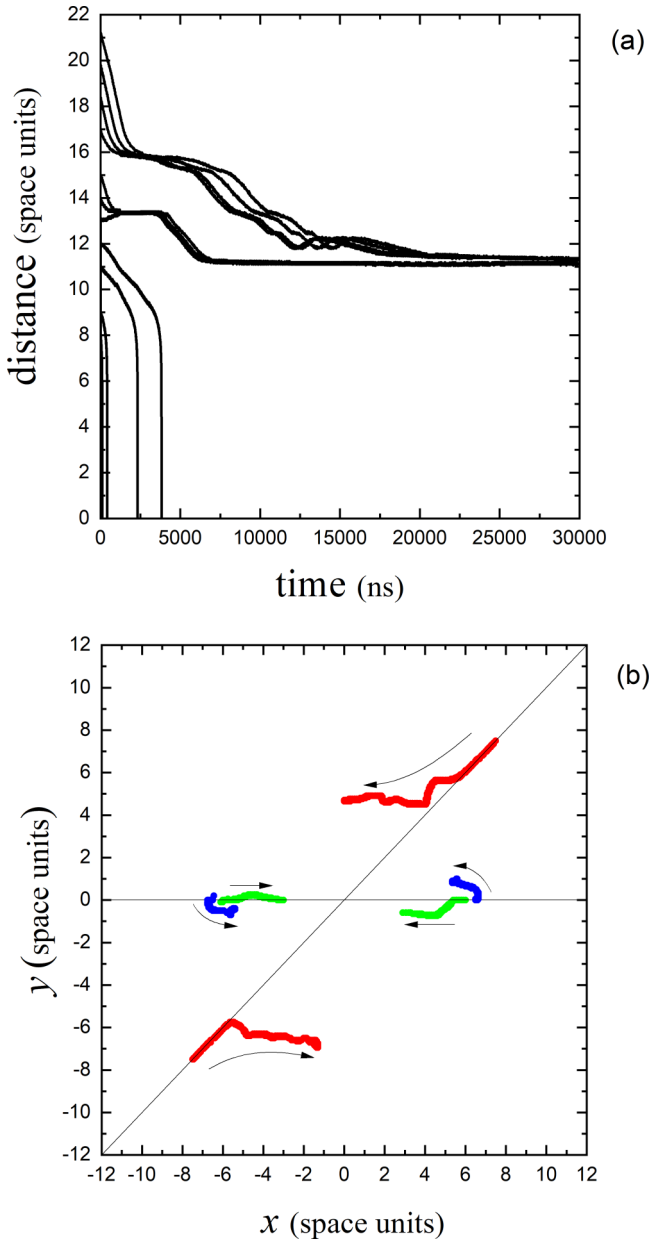

FIG. 2. Interaction of two CSs close to the locking point ($|E_{HB}|^2 = 0.9$). (a) Time evolution of the distance of pairs of CSs with different initial distance; (b) trajectory of the CSs for initial distance equal to 21.21 (red), 13 (blue), and 12 (green).

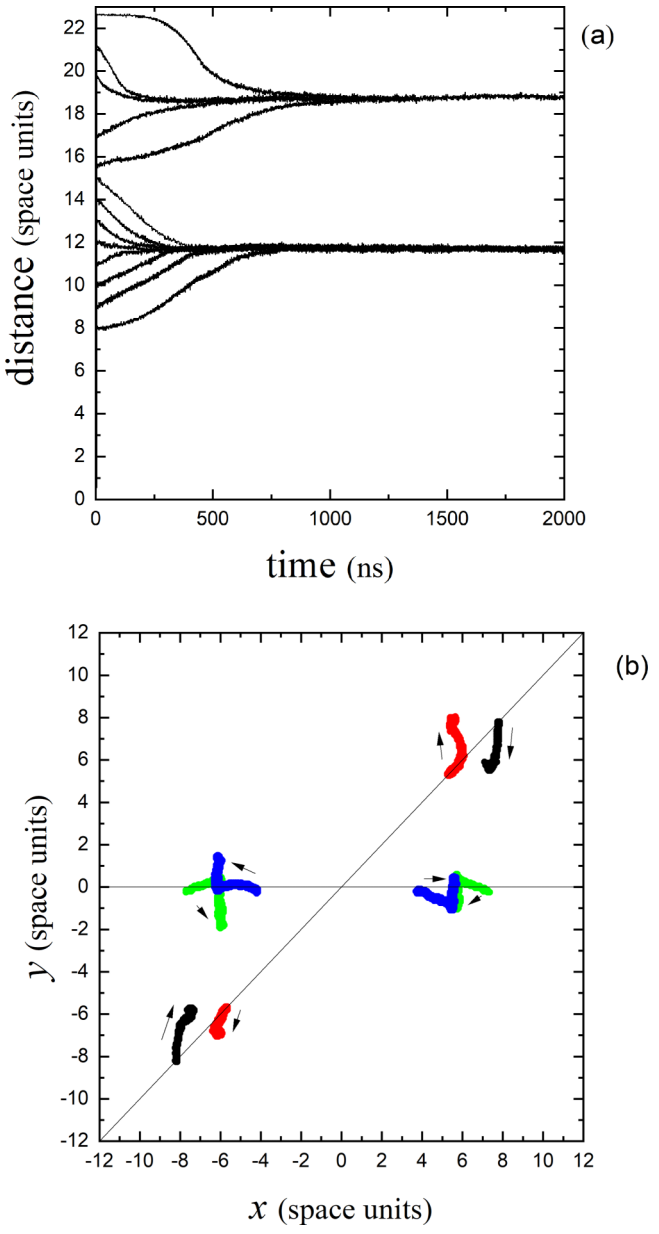

FIG. 3. Interaction of two CSs far from the locking point ($|E_{HB}|^2 = 0.75$). (a) Time evolution of the distance of pairs of CSs with different initial distance; (b) trajectory of the CSs for initial distance equal to 21.21 (black), 15.56 (red), 15 (green), and 8 (blue). The CSs merge when the initial distance is smaller than 8 s.u.

towards each other as in Ref. [26] but then they deviate and start moving approximately along a circumference in opposite direction, until they stop when they reach the equilibrium distance. For the smaller initial distance there is only a small counterclockwise motion of the two CSs.

Figure 3 shows the interaction of the two CSs in the middle of the Hopf region, for $|E_{HB}|^2 = 0.75$. The behavior differs from that of the previous case under several respects.

For initial distances larger than or equal to 8 s.u. the CSs do not merge. For smaller initial distances they merge but the motion is so fast (some tens of ns) that we do not plot it in Fig. 3 because it would be hardly visible on that time scale.

Two equilibrium distances are found instead of one, and the distance increases or decreases depending on the initial value. When the initial distance is between 8 and 15 s.u. the final equilibrium distance is 11.7 s.u. For initial distance between 15.56 and 21.21 s.u. the final equilibrium distance is 18.7 s.u.

For this value of the intensity of the holding beam the equilibrium distance is reached much more rapidly than in the previous case. We can conclude that the presence of a highly unstable background makes the dynamics faster and prevents the CSs from merging, unless they are already very close to each other at the beginning.

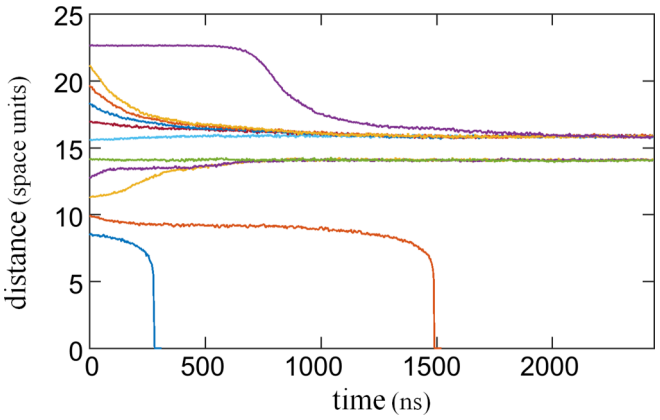

FIG. 4. Interaction of two CSs far from the locking point ($|E_{HB}|^2 = 0.75$) according to the reduced set of equations (5) and (6). The plot shows the time evolution of the distance of pairs of CSs with different initial distance. The CSs merge when the initial distance is smaller than or equal to 10 s.u.

IV. REDUCED DYNAMICAL EQUATIONS

The numerical simulations of the previous section were based on the full set of dynamical equations (1)–(3), which include the macroscopic polarization P. The presence of the fast variable P makes the equations stiff and slows down the numerical simulations. If the polarization P is adiabatically eliminated setting $\dot{P} = 0$ we obtain the reduced set of equations

$$\dot{E} = \sigma[E_{HB} - (1 + i\theta)E + (1 - i\alpha)(1 - \beta D)DE + i\nabla^2 E], \tag{5}$$

$$\dot{D} = \mu - D - (1 - \beta D)D|E|^2 + d_D\nabla^2 D, \tag{6}$$

which are the same equations used in Ref. [26]. Physically, the adiabatic elimination of P amounts to assuming that the gain is flat. In Ref. [26] such an approximation was valid because the simulations were limited to values of the amplitude of the holding beam above the injection locking point, where the CSs are stationary, or quasistationary since they move slowly one towards the other, and the background is stable. In such conditions only the transverse modes with small wave vectors are excited and the assumption of flat gain has no effects.

Here, instead, we are considering values of the amplitude of the holding beam below the injection locking point, where the background is unstable. The assumption of flat gain in this case implies that all the unstable transverse modes with any value of the transverse wave vector experience the same gain. In principle this would lead to the unphysical growth of modes with infinitely small wavelength. In the numerical simulations this does not occur because the finiteness of the integration grid sets an upper limit to the transverse wave vector, but what we observe is the formation of unphysical spatial structures in the background with a spatial scale equal to the period of the spatial grid, as shown in the upper panel of Fig. 5.

Although we are aware of the limitations of the model (5) and (6) for a laser below the injection locking point, we repeated the simulations of Fig. 3 in order to ascertain if and how such an unphysical behavior of the background

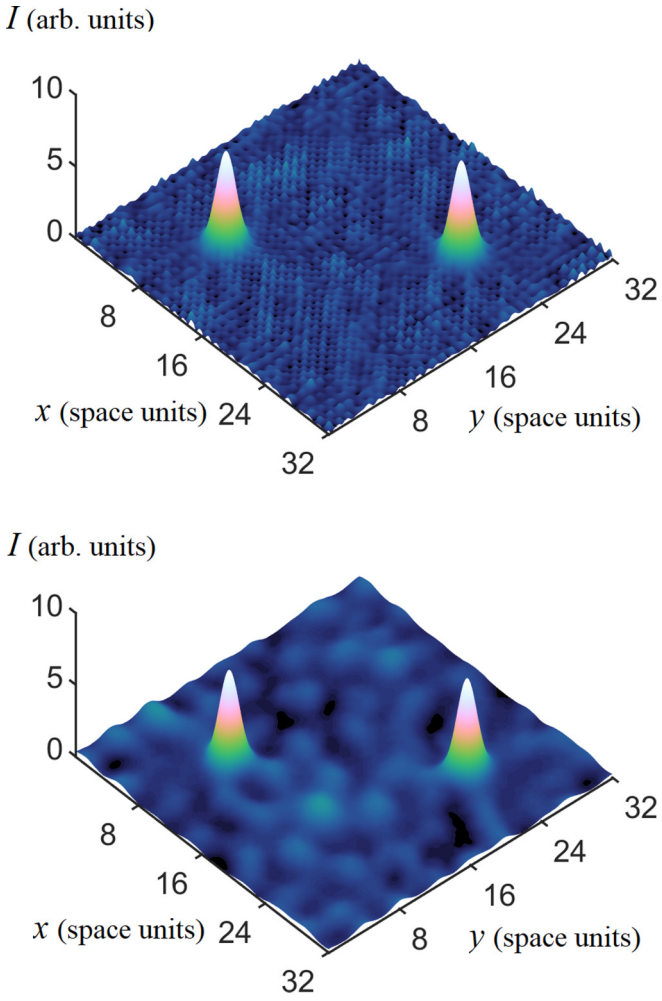

FIG. 5. Three dimensional plots of the field intensity in the transverse plane when two CSs are switched on along the diagonal of the integration window at a distance of approximately 20 s.u. The upper panel was obtained with the reduced equations (5) and (6) and shows the formation of irregular spatial structure with the same period of the integration grid. In the lower panel, instead, Eq. (5) was substituted with Eq. (7) which contains a diffusion term which damps the larger transverse wave vectors and regularizes the dynamics of the background.

affects the interaction of the CSs. The results are shown in Fig. 4. Two major differences emerge. First, the CSs merge even for initial distances for which in Fig. 3 they move apart and reach an equilibrium distance. Second, although we still have two equilibrium distances for most initial distances, such equilibrium distances are much different from those found using the full set of equations (1), (2), and (3).

Therefore, we conclude that indeed the reduced equations (5) and (6) are not suitable to simulate the dynamics of interacting CSs below the injection locking point.

However, an easy way to account for the finite gain linewidth without resorting to the full set of equations (1), (2), and (3) consists in adding a diffusion term in the equation for the field, i.e., in adding a real part d_E to the imaginary coefficient of the Laplacian. Here the additional diffusive term has been introduced phenomenologically, although a

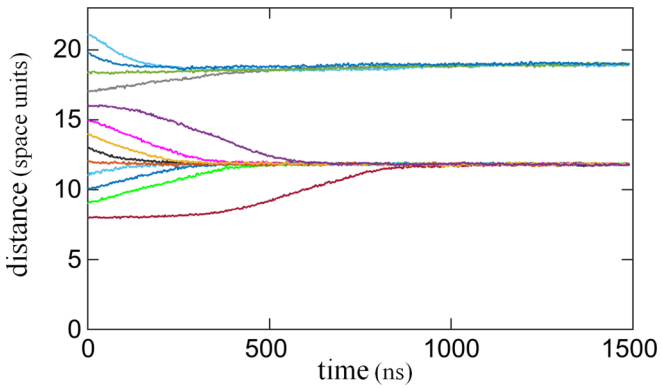

FIG. 6. Interaction of two CSs far from the locking point ($|E_{HB}|^2 = 0.75$) according to the reduced set of equations (7) and (6) and $d_E = 7.5 \times 10^{-4}$. The plot shows the time evolution of the distance of pairs of CSs with different initial distance. The CSs never merge for an initial distance larger than or equal to 8 s.u.

detailed derivation can be found in Ref. [15] for a two-level system and in Ref. [32] for a VCSEL. In general, a refined adiabatic elimination of the polarization which goes beyond simply setting its time derivative equal to zero introduces new terms in the remaining equations, some of them acting as spectral filters, thus mimicking the finite gain bandwidth of the medium.

The equation for the field E reads

$$\dot{E} = \sigma[E_{HB} - (1 + i\theta)E + (1 - i\alpha)(1 - \beta D)DE + (d_E + i)\nabla^2 E], \tag{7}$$

and the effect of the diffusion term is that of adding a damping term $-\sigma d_E k^2 E_k$ to any transverse mode E_k with transverse wave vector of modulus k. The diffusion term can therefore also be interpreted as a loss term for modes that propagate in an oblique direction in a transversely finite cavity [33].

We determined the best value of the phenomenological diffusion coefficient d_E by imposing that using Eqs. (7) and (6) with the parameters of Fig. 2, i.e., $E_{HB}^2 = 0.9$, we obtain for the smaller initial distances approximately the same merging times as with the full set of equations. Proceeding in that way we found the value $d_E = 7.5 \times 10^{-4}$, which then we used to repeat the simulations of Fig. 3. In the lower panel of Fig. 5 we can see that the addition of the diffusion term is enough to regularize the spatiotemporal dynamics of the background, which now occurs on a larger spatial scale.

The time evolution of the distance displayed in Fig. 6 shows a much better agreement with the full model than that of Fig. 4. Now the CSs never merge for the considered initial distances and the values of the equilibrium distances are also very close to that of Fig. 3. The only noticeable difference consists in the slightly different value of the critical initial distance that separates the two sets evolving to the two equilibrium distances. Such a critical distance is larger in Fig. 6.

V. CONCLUSIONS

We have studied the interaction of two CSs in a driven VCSEL above lasing threshold when the laser is operated below the injection locking point, and compared it to that recently observed in the same system operated above such a point [26]. In the latter case, it was shown that the CSs always merge, independent of the initial distance. Here we show that, if the laser is below but close to the injection locking point, the CSs still merge, but only when the initial distance is below a certain value. Above that value they move until they reach an equilibrium distance, which is the same for all initial distances. If we decrease the intensity of the holding beam so that the laser is farther from the injection locking point, the CSs do not merge any more, unless they are initially very close to each other, and they repel or attract until they reach two possible equilibrium distances.

The reason for the existence of equilibrium distances here cannot be attributed to the same dynamical mechanisms at the origin of the formation of clusters of stationary dissipative solitons [27,28] or oscillatory solitons [29], because here we do not observe any oscillatory tail in the surroundings of the CS peak, neither when they are stationary (that is, for injection intensity above the injection locking point) nor when they sit on a turbulent background (that is the case presented here, for injection intensity below the injection locking point).

The dynamics of the CSs is modeled by a set of effective Maxwell-Bloch equations where the presence of an equation for the macroscopic polarization P allows one to avoid the short wavelength oscillatory instability which instead affects the reduced model obtained with the adiabatic elimination of P. While such a model is suitable to study the dynamics of the CSs above the injection locking point, as in Ref. [26], here we show that below the injection locking point it leads to incorrect predictions. However, the results of the complete model are recovered without increasing the complexity of the model by simply adding a diffusion term in the equation for the electric field.

[1] S. Wieczorek, B. Krauskopf, and D. Lenstra, Opt. Commun. **172**, 279 (1999).
[2] J. R. Tredicce, F. T. Arecchi, G. L. Lippi, and G. P. Puccioni, JOSA B **2**, 173 (1985).
[3] T. Ackemann, W. J. Firth, and G. L. Oppo, Adv. At., Mol., Opt. Phys. **57**, 323 (2009).
[4] L. A. Lugiato, F. Prati, and M. Brambilla, *Nonlinear Optical Systems* (Cambridge University Press, Cambridge, UK, 2015).
[5] N. N. Rosanov and G. V. Khodova, J. Opt. Soc. Am. B **7**, 1057 (1990).
[6] M. Brambilla, L. A. Lugiato, F. Prati, L. Spinelli, and W. J. Firth, Phys. Rev. Lett. **79**, 2042 (1997).
[7] L. Spinelli, G. Tissoni, M. Brambilla, F. Prati, and L. A. Lugiato, Phys. Rev. A **58**, 2542 (1998).
[8] S. Barland, J. R. Tredicce, M. Brambilla, L. A. Lugiato, S. Balle, M. Giudici, T. Maggipinto, L. Spinelli, G. Tissoni, T. Knoedl *et al.*, Nature (London) **419**, 699 (2002).

[9] X. Hachair, S. Barland, L. Furfaro, M. Giudici, S. Balle, J. R. Tredicce, M. Brambilla, T. Maggipinto, I. M. Perrini, G. Tissoni *et al.*, Phys. Rev. A **69**, 043817 (2004).
[10] G. L. Oppo, G. D'Alessandro, and W. J. Firth, Phys. Rev. A **44**, 4712 (1991).
[11] X. Hachair, F. Pedaci, E. Caboche, S. Barland, M. Giudici, J. R. Tredicce, F. Prati, G. Tissoni, R. Kheradmand, L. A. Lugiato *et al.*, IEEE J. Sel. Top. Quantum Electron. **12**, 339 (2006).
[12] M. Eslami, R. Kheradmand, and K. M. Aghdami, Phys. Scr. **2013**, 014038 (2013).
[13] W. J. Firth and A. J. Scroggie, Phys. Rev. Lett. **76**, 1623 (1996).
[14] T. Maggipinto, M. Brambilla, G. K. Harkness, and W. J. Firth, Phys. Rev. E **62**, 8726 (2000).
[15] S. V. Fedorov, A. G. Vladimirov, G. V. Khodova, and N. N. Rosanov, Phys. Rev. E **61**, 5814 (2000).
[16] F. Prati, G. Tissoni, L. A. Lugiato, K. M. Aghdami, and M. Brambilla, Eur. Phys. J. D **59**, 73 (2010).
[17] N. N. Rosanov, S. V. Fedorov, and A. N. Shatsev, Appl. Phys. B: Lasers Opt. **81**, 937 (2005).
[18] N. N. Rosanov, S. V. Fedorov, and N. A. Veretenov, Eur. Phys. J. D **73**, 141 (2019).
[19] G. Tissoni, K. M. Aghdami, M. Brambilla, and F. Prati, Eur. Phys. J.: Spec. Top. **203**, 193 (2012).
[20] F. Pedaci, P. Genevet, S. Barland, M. Giudici, and J. R. Tredicce, Appl. Phys. Lett. **89**, 221111 (2006).
[21] F. Pedaci, S. Barland, E. Caboche, P. Genevet, M. Giudici, J. R. Tredicce, T. Ackemann, A. J. Scroggie, W. J. Firth, G. L. Oppo *et al.*, Appl. Phys. Lett. **92**, 011101 (2008).
[22] F. Prati, G. Tissoni, C. McIntyre, and G. L. Oppo, Eur. Phys. J. D **59**, 139 (2010).
[23] L. Spinelli, G. Tissoni, L. A. Lugiato, and M. Brambilla, Phys. Rev. A **66**, 023817 (2002).
[24] A. J. Scroggie, J. M. McSloy, and W. J. Firth, Phys. Rev. E **66**, 036607 (2002).
[25] R. Kheradmand, L. A. Lugiato, G. Tissoni, M. Brambilla, and H. Tajalli, Opt. Express **11**, 3612 (2003).
[26] S. R. Anbardan, C. Rimoldi, R. Kheradmand, G. Tissoni, and F. Prati, Phys. Rev. E **97**, 032208 (2018).
[27] B. Schäpers, M. Feldmann, T. Ackemann, and W. Lange, Phys. Rev. Lett. **85**, 748 (2000).
[28] A. G. Vladimirov, J. M. McSloy, D. V. Skryabin, and W. J. Firth, Phys. Rev. E **65**, 046606 (2002).
[29] D. Turaev, A. G. Vladimirov, and S. Zelik, Phys. Rev. Lett. **108**, 263906 (2012).
[30] H. Vahed, R. Kheradmand, H. Tajalli, G. Tissoni, L. A. Lugiato, and F. Prati, Phys. Rev. A **84**, 063814 (2011).
[31] M. Eslami, R. Kheradmand, and G. Hashemvand, Opt. Quantum Electron. **46**, 319 (2014).
[32] G. L. Oppo, A. M. Yao, F. Prati, and G. J. deValcárcel, Phys. Rev. A **79**, 033824 (2009).
[33] N. N. Rosanov, S. V. Fedorov, L. A. Nesterov, and N. A. Veretenov, Nanomaterials **9**, 826 (2019).